# Isomer-resolved unimolecular dynamics of the hydroperoxyalkyl intermediate (•QOOH) in cyclohexane oxidation

Yujie Qian<sup>a</sup>, Tarun Kumar Roy<sup>a</sup>, Ahren W. Jasper<sup>b</sup>, Christopher A. Sodjak<sup>a</sup>, Marisa C. Kozlowski<sup>a</sup>, Stephen J. Klippenstein<sup>b,\*</sup> and Marsha I. Lester<sup>a,\*</sup>

# ORCID IDs

Y. Qian 0000-0001-7799-3096 T. K. Roy 0000-0003-3181-7067 A. W. Jasper 0000-0003-0216-9347 C. A. Sodjak 0000-0002-1176-6736 M. C. Kozlowski 0000-0002-4225-7125 S. J. Klippenstein 0000-0001-6297-9187 M. I. Lester 0000-0003-2367-3497

 <sup>&</sup>lt;sup>a</sup> Department of Chemistry, University of Pennsylvania, Philadelphia, PA 19103-6323 USA
<sup>b</sup> Chemical Sciences and Engineering Division, Argonne National Laboratory, Lemont, IL
60439, USA

<sup>\*</sup> Corresponding author Marsha I. Lester, <u>milester@sas.upenn.edu</u>; co-corresponding author Stephen J. Klippenstein, <u>sik@anl.gov</u>.

## Abstract

The oxidation of cycloalkanes is important in combustion of transportation fuels and atmospheric secondary organic aerosol formation. A transient carbon-center radical intermediate ( $\bullet$ QOOH) in the oxidation of cyclohexane is identified through its infrared fingerprint and time- and energy-resolved unimolecular dissociation dynamics to hydroxyl (OH) radical and bicyclic epoxide products. Although the cyclohexyl ring structure leads to three nearly degenerate  $\bullet$ QOOH isomers ( $\beta$ -,  $\gamma$ - and  $\delta$ -QOOH), their transition state barriers to OH products differ considerably. Selective characterization of the  $\beta$ -QOOH isomer is achieved at excitation energies associated with the lowest transition state barrier leading to OH products that are detected. A benchmarking approach is employed for calculation of high accuracy stationary point energies, in particular transition state barriers, for cyclohexane oxidation ( $C_6H_{11}O_2$ ), building on higher level reference calculations for the smaller  $C_2H_5O_2$  system. The isomer specific characterization of  $\beta$ -QOOH is validated by comparison of experimental OH product appearance rates with computed statistical microcanonical rates, including significant heavy atom tunneling, at energies in the vicinity of the transition state barrier. Master-equation modeling is utilized to extend the results to thermal unimolecular decay rate constants at temperatures and pressures relevant to cyclohexane combustion.

Classification: Physical Science, Chemistry

Keywords: hydroperoxyalkyl intermediate, unimolecular decay, transition state barriers, cyclohexane oxidation, combustion and atmospheric chemistry

Significance statement: Carbon-centered radicals with a hydroperoxy (-OOH) group, commonly known as •QOOH, are a rarely observed, yet critical, intermediate species in hydrocarbon oxidation processes relevant to combustion and atmospheric chemistry. A •QOOH intermediate in the oxidation of cyclohexane is directly observed, revealing its infrared fingerprint and time- and energy-resolved dissociation to hydroxyl radical (OH) products. The experimental results are complemented by high-level electronic structure calculations, which implement a benchmarking approach to improve the accuracy of electronic energies and computed dissociation rates for larger systems.

### Introduction

Cycloalkanes are important from a combustion perspective because they are a significant component of conventional<sup>1,2</sup> and alternative<sup>3-5</sup> transportation fuels, although low temperature oxidation of cycloalkanes is generally less efficient than that for acyclic alkanes of similar size.<sup>6</sup> The emission and subsequent oxidation of cycloalkanes in the atmosphere is also important because their yields of secondary organic aerosols (SOA) are much greater than those of corresponding size linear or branched alkanes.<sup>7-9</sup> Their overall contribution to SOA formation in an urban environment was recently proposed to exceed that from linear alkanes.<sup>10</sup>

Cyclohexane is considered to be a model saturated cyclic hydrocarbon and has been the focus of numerous experimental studies of combustion<sup>11</sup> and atmospheric<sup>12, 13</sup> oxidation processes. Theoretical calculations have also been employed in development of detailed kinetic models.<sup>6, 14-17</sup> Most recently, low temperature oxidation experiments utilizing jet-stirred reactors combined with photoionization mass spectrometric identification of products have been combined with quantum chemical calculations and master equation kinetic modeling to examine the primary oxidation mechanism of cyclohexane.<sup>17-19</sup> Structural differences provide an interesting contrast between cyclic alkanes and more extensively investigated linear and/or branched alkanes. For example, the cyclohexyl ring imposes structural constraints not present for linear and branched hydrocarbons that give rise to bicyclic transition states and products.<sup>15, 16</sup> There are also multiple isomeric products originating from distinct cyclohexyl ring sites and conformations, which complicate interpretation of kinetic measurements.

Critical intermediates along the oxidation pathway of cyclic hydrocarbons have remained unexplored in prior experimental studies. The present investigation employs infrared action spectroscopy and detailed theoretical analyses to obtain an infrared spectroscopic signature of a transient carbon-centered hydroperoxyalkyl radical intermediate (•C<sub>6</sub>H<sub>10</sub>OOH) in the oxidation of cyclohexane, and its time- and energy-resolved dissociation dynamics to hydroxyl radical (OH) and bicyclic epoxide products. The experimental microcanonical rate constants obtained for a specific isomer are also utilized to validate a benchmarking approach for calculating accurate stationary point energies, in particular transition state (TS) barriers, in the oxidation of cyclohexane and larger systems.

The general chain reaction sequence for hydrocarbon (RH) oxidation and that specific to cyclohexane oxidation are illustrated in Figure 1. The oxidation of cyclohexane is initiated by reaction with OH radicals (or other radicals such as HO<sub>2</sub>) through H-atom abstraction, forming a carbon-centered cyclohexyl radical (R•) that rapidly reacts with O<sub>2</sub> (first O<sub>2</sub> addition) to generate cyclohexyl-peroxy radicals (ROO•). ROO• then isomerizes through intramolecular H-atom transfer to produce the carbon-centered hydroperoxy-cyclohexyl radical (•QOOH), composed of a hydroperoxide group (-OOH) and a new carbon radical center (•Q) at several distinct sites on the cyclohexyl ring. The •QOOH

intermediates can be transiently stabilized and/or dissociate to release OH radical and multiple bicyclic epoxide (or hexenal) products, thereby facilitating OH radical chain propagation.<sup>22</sup> Alternatively, •QOOH can revert back to ROO• via internal H abstraction or undergo direct HO<sub>2</sub> elimination to alkene products (effectively chain terminating). The elusive •QOOH reaction intermediates are the 'central switchyard' in the chain reaction mechanism,<sup>23</sup> and are therefore a critical target requiring experimental characterization of their structure, stability, and decay dynamics.

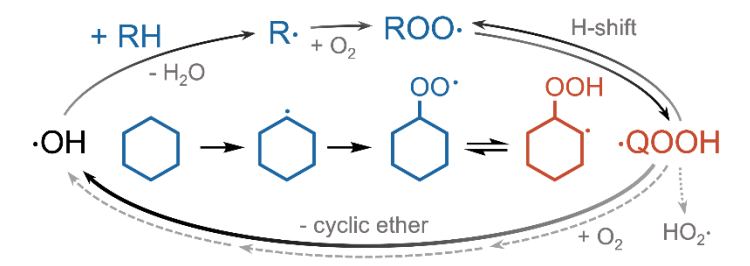


**Figure 1**. Overview of hydrocarbon oxidation mechanism (outer ring) and that specific to cyclohexane oxidation (central). In general, a volatile hydrocarbon (RH) reacts with OH radicals to form hydrocarbon radicals (R•) that rapidly react with atmospheric O<sub>2</sub> to yield alkyl peroxy radicals (ROO•), followed by a H-shift to a transient carbon-centered •QOOH radical. The •QOOH radical can undergo unimolecular decay to regenerate OH radicals with a cyclic ether, revert back to ROO• via H-shift, dissociate to HO<sub>2</sub> + alkene (dotted), or add a second O<sub>2</sub> for further oxidation (dashed). The OH initiated oxidation of cyclohexane to cyclohexyl, O<sub>2</sub> addition to form cyclohexyl-peroxy, and H-atom transfer to produce •QOOH radicals are also depicted in the central region.

Unimolecular decomposition of •QOOH typically competes against its bimolecular reaction with  $O_2$  (second  $O_2$  addition) to form oxygen-centered peroxy radicals •OOQOOH. In low-temperature combustion, the •OOQOOH radicals can undergo another internal hydrogen-atom transfer to HOOP•OOH, which dissociates to a OH radical and ketohydroperoxide (KHP, HOOP=O). (The  $R \rightarrow Q \rightarrow P$  notation indicates one fewer C-H bond in each step.) Subsequent decomposition of KHP to a second OH radical along with a •OP=O radical gives rise to chain branching.<sup>23, 24</sup> In atmospheric chemistry, repeated cycles of hydrogen shifts (ROO• to •QOOH) and  $O_2$  addition (to form •OOQOOH) occur during oxidation of abundant volatile organic compounds, such as isoprene and  $\alpha,\beta$ -pinene, leading to more highly oxidized and lower volatility species.<sup>25-28</sup> Atmospheric oxidation of isoprene has also been shown to proceed via a  $\beta$ -QOOH radical to yield epoxides (cyclic ethers),<sup>25, 29, 30</sup> a precursor to secondary organic aerosol formation, along with regeneration of OH radicals.

Direct experimental observations of •QOOH radicals are extremely limited, <sup>31-33</sup> although there has been extensive theoretical characterization of their properties. <sup>34-36</sup> Instead, most prior experimental studies have focused on product characterization and indirect kinetic measurements associated with •QOOH chemistry. <sup>15, 19, 31, 37-39</sup> The fundamental difficulty in directly observing •QOOH intermediates arises from their low steady-state concentrations due to slow formation at low temperatures and rapid

removal reactions that include unimolecular decomposition and barrierless reaction with O<sub>2</sub>. To date, Savee et al. reported observation of a resonantly stabilized •QOOH radical formed in the oxidation of 1,3-cycloheptadiene.<sup>31</sup> The resonance stabilization in this system increased the stability of the •QOOH radical and substantially raised the barrier for its unimolecular decomposition to OH products (~30 kcal mol<sup>-1</sup>) compared to the approximately threefold lower barriers predicted for a wide range of •QOOH radicals.<sup>34</sup> Recently, this laboratory characterized a prototypical •QOOH radical formed in oxidation of isobutane [•CH<sub>2</sub>(CH<sub>3</sub>)<sub>2</sub>COOH] with barrier to unimolecular decay of only 10.3 kcal mol<sup>-1</sup>.<sup>32, 33</sup>

# **Results**

The present study identifies a hydroperoxy-cyclohexyl radical intermediate (•C<sub>6</sub>H<sub>10</sub>OOH; hereafter denoted as •QOOH) and characterizes a bicyclic transition state associated with cyclohexane oxidation. This is achieved by laboratory generation and stabilization of the •QOOH intermediate under supersonic jet-cooled conditions, and identification of •QOOH through its infrared spectroscopic fingerprint. Infrared activation also initiates time- and energy-dependent unimolecular decay of •QOOH, leading to OH products that are detected. The measured rates for appearance of OH products are compared with complementary microcanonical rate calculations, which provides a sensitive probe of the properties of the transition state barrier leading to OH + bicyclic ether products. These calculations also help demonstrate the isomer specificity of the experimental observations.

The OH initiated oxidation of cyclohexane is more complicated than our prior study on isobutane oxidation because it can lead to •QOOH radicals with three distinct radical sites on the cyclohexyl ring:  $\beta$ -,  $\delta$ -, and  $\gamma$ -QOOH isomers. <sup>15-17, 40</sup> Theoretical calculations have shown that  $\alpha$ -QOOH radicals are not stable, <sup>41</sup> in this case immediately dissociating to OH + cyclohexanone. <sup>6, 16, 42</sup> The  $\beta$ -,  $\delta$ -, and  $\gamma$ -QOOH isomers have similar stabilities that differ from one another by only ca. 1 kcal mol<sup>-1</sup> (relative to cyclohexyl + O<sub>2</sub>). <sup>15-17</sup> However, the transition state (TS) barriers along the reaction pathways from  $\beta$ -,  $\gamma$ -, and  $\delta$ -QOOH to OH + co-products (generally, bicyclic epoxides) are predicted to differ considerably from one another as shown in Figure 2.

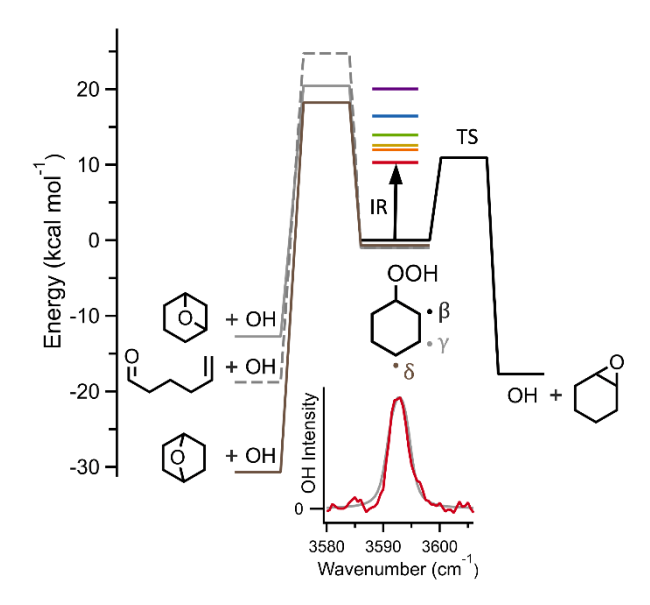


**Figure 2**. Reaction pathways for unimolecular decay of carbon-centered hydroperoxy-cyclohexyl radicals (•QOOH) to OH radical products. The carbon radical site of •QOOH can be located at the  $\beta$ ,  $\gamma$ , or  $\delta$  cyclohexyl ring position, leading to reaction pathways with distinct transition state (TS) barriers to OH + cyclic ether or hexenone products (Table ST3). The reaction pathways for the •QOOH isomers are denoted as follows: β-QOOH (black),  $\gamma$ -QOOH (solid and dashed gray), and  $\delta$ -QOOH (brown). Experimental studies of jet-cooled and isolated •QOOH radicals are initiated by IR activation at specific energies in the 3500 to 7000 cm<sup>-1</sup> spectral region (denoted by red to purple color coding), corresponding to excitation energies of 10-20 kcal mol<sup>-1</sup>, resulting in time-resolved unimolecular decay to OH products that are detected by UV laser-induced fluorescence (LIF). Only  $\beta$ -QOOH will result in facile unimolecular decay to OH products at these excitation energies. The inset shows the fundamental OH stretch ( $\nu$ <sub>OH</sub>) of jet-cooled  $\beta$ -QOOH at 3593.0 cm<sup>-1</sup> (10.27 kcal mol<sup>-1</sup>) acquired with LIF detection of OH products.

In this study, IR excitation in the 3500 to 7000 cm<sup>-1</sup> spectral region, corresponding to 10-20 kcal  $mol^{-1}$  excitation energy, is utilized to identify IR transitions of jet-cooled and isolated hydroperoxy-cyclohexyl radicals. Moreover, IR excitation initiates unimolecular decay of •QOOH to OH products, which are detected by UV laser-induced fluorescence (LIF).<sup>32, 43</sup> Prior theoretical studies<sup>15-17</sup> as well as the high level calculations presented herein predict that the transition state (TS) barriers leading from the three distinct carbon-centered hydroperoxy-cyclohexyl radicals,  $\beta$ -,  $\gamma$ -, and  $\delta$ -QOOH isomers, to OH products range from ca. 10 to 25 kcal  $mol^{-1}$  as shown in Figure 2. The TS barriers from  $\gamma$ - and  $\delta$ -QOOH to OH products ( $\geq$  18 kcal  $mol^{-1}$ ) are considerably higher than that leading from  $\beta$ -QOOH to OH + cyclic ether products (ca. 11 kcal  $mol^{-1}$ ), indicating that  $\beta$ -QOOH will be selectively probed at these IR excitation energies when combined with LIF detection of OH products. The reverse pathway from  $\beta$ -QOOH to the cyclohexyl-peroxy radical (ROO•, see Figure ST1) has a much higher TS barrier and is not predicted to be a significant decay channel. As a result, the combination of IR excitation in this spectral

region and time-resolved UV detection of OH products enables selective experimental observation of the  $\beta$ -QOOH isomer and its unimolecular decay dynamics to OH + 1,2-epoxy-cyclohexane (epoxycyC6-1a) products.

In the present study, •QOOH radicals are generated by H-atom abstraction from one of the CH<sub>2</sub> groups of cyclohexyl hydroperoxide (CHHP) utilizing photolytically generated Cl atoms upon 355 nm photolysis of Cl<sub>2</sub>. The H-atom abstraction reaction is carried out within a quartz capillary reactor tube affixed to a pulsed valve as in prior experiments.<sup>32, 44</sup> The newly formed  $\beta$ -,  $\gamma$ -, and/or  $\delta$ -QOOH radicals are collisionally stabilized within the capillary tube and cooled to low rotational temperature (ca. 10 K) in the ensuing supersonic expansion. By contrast, H-atom abstraction from the  $\alpha$  ring site of CHHP leads to an unstable  $\alpha$ -QOOH radical,<sup>6, 16, 41, 42</sup> which spontaneously decomposes to OH + cyclohexanone. Further details of the experimental methods are provided in Supplementary Information (SI).

The jet-cooled and stabilized •QOOH radicals are vibrationally activated utilizing IR transitions associated with fundamental OH stretch ( $\nu_{OH}$ ), combination bands involving fundamental CH or OH stretches with lower frequency modes, overtone CH stretches ( $2\nu_{CH}$ ), and overtone OH stretch ( $2\nu_{OH}$ ) in the spectral region spanning from ca. 3500 to 7000 cm<sup>-1</sup> (Table SE1). The assignment of IR transitions is guided by the IR frequencies and intensities predicted by theoretical calculations (B2PLYP-D3/cc-pVTZ level of theory). The predicted IR transitions are similar for  $\beta$ -,  $\gamma$ -, and/or  $\delta$ -QOOH radicals, each with strong fundamental and overtone OH st

retches and many weaker combination bands. For example, the fundamental OH stretch ( $v_{OH}$ ) predicted for the axial and equatorial conformers of the  $\beta$ -,  $\gamma$ -, and  $\delta$ -QOOH isomers differ from one another by only a few cm<sup>-1</sup> (Figure SE1, Table SE2). As a result, IR spectral transitions alone are not sufficient to assign the isomer. Instead, the distinctly different TS barriers from the  $\beta$ -,  $\gamma$ -, and/or  $\delta$ -QOOH radicals to OH products (Table ST3) are taken into account. Only IR activated  $\beta$ -QOOH in this spectral region will have sufficient energy to surmount the TS barrier for unimolecular decay to OH products.

A strong spectral feature observed at 3593.0 cm<sup>-1</sup> and attributed to the fundamental OH stretch ( $v_{OH}$ ) of  $\beta$ -QOOH is shown as an insert in Figure 2. The band contour can be simulated as a single rovibrational feature with a rotational temperature of ca. 10 K. The observation of a single, isolated OH stretch transition is notable, since  $\beta$ -QOOH is predicted to have two conformations with axial (0 kcal mol<sup>-1</sup>) and equatorial (0.4 kcal mol<sup>-1</sup>) orientations of the hydroperoxide (–OOH) group relative to the cyclohexyl ring with fundamental OH stretch transitions predicted at 3587.8 cm<sup>-1</sup> and 3601.3 cm<sup>-1</sup>, respectively (Table SE2). The observation of a single  $v_{OH}$  feature suggests efficient equatorial-to-axial relaxation (conformational barrier of ca. 4 kcal mol<sup>-1</sup>) during jet-cooling in the present experiment. A

strong and distinctive feature is also identified at  $7008.0 \text{ cm}^{-1}$ , and ascribed to the overtone OH stretch  $(2\nu_{OH})$  for the axial conformer of  $\beta$ -QOOH predicted at  $7000.6 \text{ cm}^{-1}$  (Table SE1). Many other IR transitions are observed in between these two features, although they are much weaker and generally appear as clusters of transitions. The  $2\nu_{OH}$  feature observed for  $\beta$ -QOOH is shifted by 4.5 cm<sup>-1</sup> to lower energy from a weak background feature resulting from by IR multiphoton excitation of the CHHP precursor at  $7012.5 \text{ cm}^{-1}$  that slowly (ca.  $1.5 \mu s$ ) releases OH products, 45 which does not depend on  $355 \mu s$ 0 mphotolysis or added Cl<sub>2</sub> gas. Addition of O<sub>2</sub> to the gas flow completely eliminated the IR-induced •QOOH ( $2\nu_{OH}$ ) signal as a result of the prompt reaction of •QOOH with O<sub>2</sub> in the reactor tube. 23,32

This work focuses on IR activation of  $\beta$ -QOOH at distinct energies from the fundamental OH stretch ( $\nu_{OH}$ ) to the overtone OH stretch ( $2\nu_{OH}$ ). In each case, intramolecular vibrational energy redistribution (IVR) is expected to be rapid (ps), leading to a statistical distribution at the specified energies. Critical insight on the unimolecular decay mechanism is obtained through direct time-resolved measurements for the appearance of OH products utilizing UV LIF detection following IR activation of  $\beta$ -QOOH. Excitation of  $\beta$ -QOOH at 3593.0 cm<sup>-1</sup> resulted in a unimolecular decay rate and corresponding appearance of OH products of  $4.6 \pm 1.6 \times 10^6$  s<sup>-1</sup> (associated lifetime of  $219 \pm 76$  ns). A representative time trace of OH LIF intensity vs. IR-UV time delay is shown as an inset in Figure 3.

IR excitation at 4183.5 and 4398.5 cm<sup>-1</sup> in the combination band region involving CH<sub>2</sub> stretch and HCH bend ( $\nu_{\text{CH2}}+\delta_{\text{HCH}}$ ) resulted in successive increases in the unimolecular decay rate to  $1.9\pm0.6\times10^7$  s<sup>-1</sup> ( $52\pm16$  ns) and  $2.8\pm0.6\times10^7$  s<sup>-1</sup> ( $36.0\pm7.7$  ns), respectively. Excitation of a distinctive feature involving OH stretch and OOH bend ( $\nu_{\text{OH}}+\delta_{\text{OOH}}$ ) at 4868.5 cm<sup>-1</sup> resulted in a faster unimolecular decay rate of  $5.2\pm1.4\times10^7$  ( $19.3\pm5.2$  ns). IR activation at 5750.0 cm<sup>-1</sup> in the overtone CH stretch region yielded a unimolecular rate of  $1.8\pm0.7\times10^8$  s<sup>-1</sup> ( $5.6\pm2.2$  ns). At the highest IR excitation energy (7008.0 cm<sup>-1</sup>), the rate of OH appearance is limited by the combined time resolution of the IR-UV pulses, resulting in a laser-limited rise time of  $\leq 3.6\pm0.6$  ns. Overall, the observed energy-dependent rates for unimolecular decay of  $\beta$ -QOOH increased nearly 40-fold over the range of energies explored. The corresponding time traces for the appearance of OH products are shown in Figure SE2. The experimentally measured unimolecular decay rates and corresponding lifetimes for  $\beta$ -QOOH are plotted in Figure 3 with error bars representing  $\pm1\sigma$  uncertainty from repeated measurements. The OH product temporal profile decayed on a microsecond timescale (Figure SE3) arising from OH products moving out of the spatial volume probed by the UV laser, as found in many prior experiments.

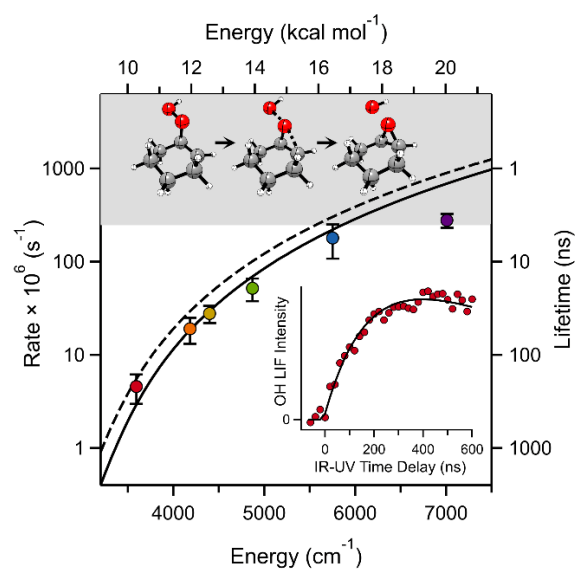


Figure 3. Energy-dependent unimolecular decay rates (with error bars representing  $\pm 1\sigma$  uncertainty from repeated measurements) and the corresponding lifetimes obtained by direct time-resolved appearance of OH products following IR activation of stabilized and jet-cooled hydroperoxy-cyclohexyl radical intermediates (β-QOOH). The color-coded points from red to purple correspond to the unimolecular rates measured with increasing IR excitation energies from 3593.0 to 7008.0 cm<sup>-1</sup> (10.3 to 20.0 kcal mol<sup>-1</sup>), respectively. The gray shaded region indicates rates or lifetimes limited by the experimental time resolution (ca. 4 ns). The inset shows a representative time trace for the appearance of OH products upon fundamental OH stretch ( $v_{OH}$ ) excitation of jet-cooled β-QOOH at 3593.0 cm<sup>-1</sup>. Statistical unimolecular decay rates are also computed based on the benchmark TS barrier of 9.49 kcal mol<sup>-1</sup> (dashed line) and optimized TS barrier of 9.76 kcal mol<sup>-1</sup> (solid line), in both cases with heavy atom tunneling and associated imaginary frequency of 734*i* cm<sup>-1</sup>. The benchmark TS barrier overestimates the rates slightly, while excellent agreement with experiment is achieved with the optimized TS barrier of 9.76 kcal mol<sup>-1</sup>. Also shown (top) are structures of the •QOOH reactant, TS barrier, and OH radical and cyclic ether (epoxycyC6-1a) products, illustrating the simultaneous O-O bond elongation and C-C-O angle contraction at the TS barrier.

The energy-resolved unimolecular decay rates measured experimentally for jet-cooled  $\beta$ -QOOH are next compared with theoretically predicted rates for  $\beta$ -QOOH to its lowest energy OH + cyclic ether (epoxycyC6-1) dissociation channel. This provides a quantitative test of RRKM theory and the barrier height predicted by theory. High level estimates of the stationary point energies on the  $C_6H_{11}O_2$  potential energy surface were determined with the CCSD(T)-F12 approach (explicitly correlated coupled cluster theory with singles, doubles, and perturbative triples) employing the cc-pVTZ-F12 basis set, following initial determination of optimized structures and zero-point energies with the B2PLYP-D3 density functional for the cc-pVTZ basis set, yielding a TS barrier of 10.86 kcal mol<sup>-1</sup>. Unfortunately, the number of heavy atoms in this system has precluded using even higher-level electronic structure methods.

Instead, benchmark calculations were undertaken for the structurally similar, yet smaller, β-QOOH system of •CH<sub>2</sub>CH<sub>2</sub>OOH. The stationary point energies for the C<sub>2</sub>H<sub>5</sub>O<sub>2</sub> radical oxidation system were determined at a higher level, which involved determination of CCSD(T)-F12/CBS-F12(TZ-F12,QZ-

F12)//CCSD(T)-F12/cc-pVTZ-F12 electronic energies together with harmonic zero point corrections as well as higher order corrections in the electronic structure calculations. These higher accuracy energies were used to improve the accuracy of the CCSD(T)-F12/cc-pVTZ-F12//B2PLYPD3/cc-pVTZ based energies using a benchmarking approach<sup>47</sup> as detailed in SI. In the smaller  $C_2H_5O_2$  system, the benchmark calculation deviated most strongly from the reference calculation for the TS barrier associated with conversion from •CH<sub>2</sub>CH<sub>2</sub>OOH to OH + oxirane ( $C_2H_4O$ , cyclic ether), specifically by reducing the TS barrier by 1.37 kcal mol<sup>-1</sup> (Table ST4). This is precisely the TS barrier of primary interest in the experimental investigation of  $\beta$ -QOOH to OH + epoxycyC6-1 in the  $C_6H_{11}O_2$  system, which in both systems involves formation of an OH radical and three-membered CCO ring product. An analogous reduction in this TS barrier was adopted for  $C_6H_{11}O_2$ , based on the assumption that the error in the reference method is equivalent for chemically related stationary points in different systems, <sup>48</sup> which lowers the TS barrier to 9.49 kcal mol<sup>-1</sup> (Table ST5). A further small adjustment of +0.27 kcal mol<sup>-1</sup> in the TS barrier, consistent with an estimated  $2\sigma$  uncertainty of ~0.6 kcal mol<sup>-1</sup>, yielded the best agreement with the experiment as described below.

The benchmark calculations for  $C_2H_5O_2$  also suggested an error in the imaginary frequency, which is important in predicting the tunneling correction to the rate constant for •CH<sub>2</sub>CH<sub>2</sub>OOH to OH + oxirane. In this case, the benchmark CCSD(T)-F12/cc-pVTZ-F12 calculation predicted a reduction in the imaginary frequency compared to the reference B2PLYP-D3//cc-PVTZ calculation by 242i cm<sup>-1</sup> (Table ST6). An equivalent shift in imaginary frequency was applied to the corresponding TS in the C<sub>6</sub>H<sub>11</sub>O<sub>2</sub> system. Specifically, the reference B2PLYP-D3//cc-PVTZ calculation for  $\beta$ -QOOH to OH + epoxycyC6–1 yielded an imaginary frequency of 976i cm<sup>-1</sup>, which was reduced to 734i cm<sup>-1</sup> (Table ST7). In both systems, the reaction coordinate is associated with simultaneous O-O bond elongation and C-C-O angle contraction at the transition state, and thus heavy atom motions give rise to tunneling.

The benchmark electronic structure calculations for  $\beta$ -QOOH to OH + epoxycyC6-1 with TS barrier of 9.49 kcal mol<sup>-1</sup>, along with the optimized TS barrier of 9.76 kcal mol<sup>-1</sup>, and 734*i* cm<sup>-1</sup> imaginary frequency were utilized for statistical Rice-Ramsperger-Kassel-Marcus (RRKM) calculations of the energy-dependent unimolecular decay rates k(E) shown in Figure 3. The computed microcanonical dissociation rates k(E) with the benchmark TS barrier overestimates the rates slightly, while the optimized TS barrier yields excellent accord with the experimental rates measured for the appearance of OH products that increase by a factor of ca. 40 over the energy range from ca. 10 to 16.5 kcal mol<sup>-1</sup>. Moreover, the imaginary tunneling frequency associated with a combination of O-O stretch and C-C-O bend coordinates results in a substantial heavy-atom tunneling enhancement of the unimolecular decay rate by a factor of 3 near threshold. Comparison of the predicted unimolecular rates with and without heavy atom tunneling in Figure ST3 (Table ST8) shows a tunneling enhancement of ca. 20% or more over

a broad range of energies as much as 9 kcal mol<sup>-1</sup> above the barrier (ca. 18.5 kcal mol<sup>-1</sup>), demonstrating the importance of heavy atom tunneling in the unimolecular decay of  $\beta$ -QOOH.

Having shown the effectiveness of benchmark calculations in evaluation of stationary point energies for  $\beta$ -QOOH to OH + epoxycyC6-1a products, we sought to extend the approach to other potential product channels in the C<sub>6</sub>H<sub>11</sub>O<sub>2</sub> system, specifically the transition state associated with H-atom transfer from β-QOOH to ROO• and that for β-QOOH dissociation to cyclohexanone + HO<sub>2</sub> (Figure ST1; Table ST5). These channels are predicted to have significantly higher TS barriers at the CCSD(T)-F12/cc-pVTZ-F12 level (Table ST5), which are refined in the benchmark calculations to 18.5 and 15.7 kcal mol<sup>-1</sup>, respectively. Analogous benchmark calculations were performed for the imaginary frequencies associated with these alternative decay channels (Table ST7). The resultant RRKM rates for β-QOOH isomerization to ROO• and dissociation to cyclohexanone + HO<sub>2</sub> are predicted to be two or more orders of magnitude slower than that associated with OH + epoxycyC6-1 production over the experimental energy range (Figure ST6). This results in a near unity yield of OH products (Figure ST7), which are experimentally detected over the 10-20 kcal mol<sup>-1</sup> range.

The experimentally observed rates are also not consistent with the significantly slower unimolecular decay rates computed for the  $\gamma$ -QOOH or  $\delta$ -QOOH isomers of the hydroperoxy cyclohexyl radicals, which primarily favor ROO• products at the experimental energies. Specifically, unimolecular decay of  $\gamma$ -QOOH is predicted to be orders of magnitude slower than the experimentally observed OH appearance rates in the 10-20 kcal mol<sup>-1</sup> energy region and results in nearly 100% yield of ROO• products (Figures ST8 and ST9). Similarly, unimolecular decay of  $\delta$ -QOOH is computed to be significantly slower than the observed rates for production of OH and favors ROO• products at energies below 18 kcal mol<sup>-1</sup> (Figure ST10). While the OH yield is predicted to increase at higher energies, leading to favorable OH branching ratios (Figure ST11), the computed rates are many orders of magnitude slower than the experimentally observed rates. The RRKM rates computed for  $\gamma$ -QOOH and  $\delta$ -QOOH demonstrate that these isomers are not observed in the present study.

The microcanonical unimolecular rates k(E) measured experimentally and validated theoretically by first principles calculations in this study can be extended to thermal unimolecular rate constants k(T,P) at temperatures (298-800 K) and pressures (0.01 bar to high-pressure limit) relevant to cyclohexane combustion. The high-pressure limit of the thermal dissociation rate k(T,P) corresponds to a Boltzmann average of the microcanonical rates, although requiring additional averaging over rotations. The pressure dependence of •QOOH + Ar was modeled using classical trajectory-based collision outcomes and master equation calculations described in Section ST4 and detailed elsewhere. The collision rate constant Z

was derived from Lennard-Jones parameters for distance  $\sigma$ , well-depth  $\epsilon$ , and collision strength  $\alpha$  determined for the interaction potential.

The computed pressure-dependent thermal rate constants for dissociation of  $\beta$ -QOOH with Ar bath gas are shown in Figure 4 (and Figure ST13); axial and equatorial conformers of  $\beta$ -QOOH are included as both are expected to be populated under thermal conditions. The thermal rates from 298 to 1000 K are illustrated at pressures ranging from 0.01 to 100 bar with extension to the high-pressure limit, along with parameterization as modified Arrhenius fits given in Table ST9. At 298 K, the thermal rate in the high-pressure limit  $k(T,P) \sim 2 \times 10^5$  s<sup>-1</sup>, corresponding to a lifetime of 5  $\mu$ s, is enhanced nearly 2-fold due to heavy atom tunneling, but the impact of tunneling falls off with increasing temperature and becomes insignificant at 1000 K. The thermal rates of dissociation terminate above temperatures at which the rate of dissociation competes or exceeds the rate of collision-induced thermalization, such that phenomenological rate descriptions are not valid.

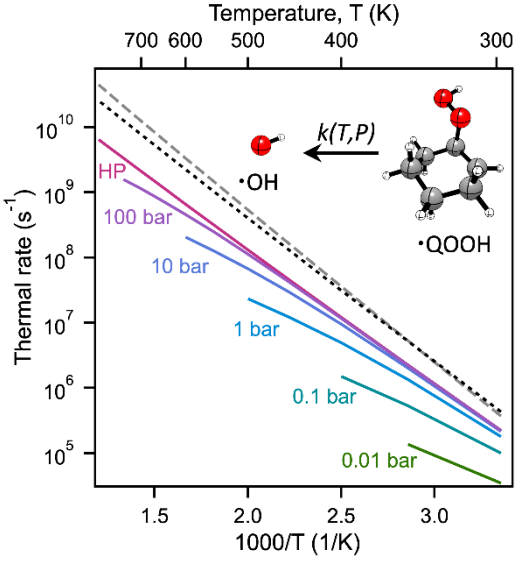


**Figure 4**. Pressure-dependent thermal rates for unimolecular dissociation of β-QOOH to OH + epoxycyC6-1 products are derived from master equation modeling. The experimentally validated TS barrier of 9.76 kcal mol<sup>-1</sup> and imaginary frequency of 734i cm<sup>-1</sup> associated with heavy atom tunneling are utilized in the master equation simulations. Phenomenological rates are not appropriate at lower pressures and higher temperatures where the thermalization and reaction timescales overlap. The temperature-dependent rates in the high-pressure (HP) limit are compared with prior theoretical predictions by Sirjean et al. (dashed gray) and Zou et al. (short dash black) in Refs. 16 and 17.

The temperature-dependent thermal rates derived for unimolecular decay of  $\beta$ -QOOH to OH + epoxycyC6-1 products in the high-pressure limit are about a factor of two to three lower than those of prior theoretical predictions by Sijean et al. <sup>16</sup> and Zou et al. <sup>17</sup> as evident in Figure 4. The predicted TS barriers (CBS-QB3) in the earlier theoretical studies are slightly higher (0.3 kcal mol<sup>-1</sup>), such that the thermal rates in the high-pressure limit should have been a little lower, not higher, than the present work.

The difference appears to originate from including only the axial conformer of  $\beta$ -QOOH in prior studies, rather than the similar population of axial and equatorial conformers anticipated under thermal conditions (e.g. 70% axial, 30% equatorial at 298 K), along with other minor discrepancies discussed in SI. Further examination of the thermal unimolecular rates for  $\beta$ -,  $\gamma$ -, and  $\delta$ -isomers of •QOOH to OH products over a wide range of temperatures from 298 to 1000 K (Figure ST14) shows that  $\beta$ -QOOH is the dominant source of OH radical products with a near unity branching to OH product in the high-pressure limit (Figure ST15). By contrast, thermal unimolecular decay starting from the cyclohexyl-peroxy radical will lead preferentially to  $\gamma$ -QOOH and a low yield of OH products in the high-pressure limit.

### **Discussion**

This investigation provides the first direct experimental observation of the hydroperoxy-cyclohexyl radical (•C<sub>6</sub>H<sub>10</sub>OOH) transiently formed in the oxidation of cyclohexane and associated cyclohexyl radicals, which is a model saturated cyclic hydrocarbon system. Theoretical studies have predicted three stable •QOOH isomers,  $\beta$ -,  $\gamma$ -, and  $\delta$ -QOOH, which have nearly degenerate energies. Isomer-specific characterization of •QOOH is realized by infrared action spectroscopy of jet-cooled samples generated by hydrogen-atom abstraction from cyclohexyl hydroperoxide. β-QOOH has a significantly lower TS barrier (9.76 kcal mol<sup>-1</sup>) leading to OH radical products than those for  $\gamma$ - or  $\delta$ -QOOH, enabling selective identification of β-QOOH upon IR activation at energies ranging from 3500 to 7000 cm<sup>-1</sup> (10 to 20 kcal mol<sup>-1</sup>) when combined with UV laser-induced fluorescence detection of OH products. The resultant energy-resolved unimolecular decay rates for β-QOOH, measured as the time-dependent appearance of OH products on a nanosecond timescale, provide a stringent test of the corresponding TS barrier. A benchmarking approach is utilized to evaluate stationary point energies – most importantly the TS barriers leading to OH products – by comparison with the structurally similar, yet smaller, β-QOOH system of •CH<sub>2</sub>CH<sub>2</sub>OOH, in which higher accuracy energies can be computed. The resultant TS barriers, after small adjustment within estimated uncertainty of the higher-level calculations, yield energy-dependent unimolecular decay rates in excellent accord with experimental measurements. Interestingly, the bicyclic TS barrier leading to OH + cyclohexanone products for  $\beta$ -QOOH in cyclohexane oxidation is ca. 0.5 kcal mol<sup>-1</sup> lower in energy than the cyclic TS characterized previously in isobutane oxidation (10.3 kcal mol<sup>-1</sup>; 763i cm<sup>-1</sup>).<sup>32</sup> Heavy atom tunneling, involving O-O extension and C-C-O angle contraction for cyclization, is again found to enhance the microcanonical unimolecular decay rates of β-QOOH by factor of 3 near threshold and by 20% or more over a broad range of energies above the TS barrier. Heavy-atom tunneling is also predicted to be relevant under thermal conditions in the high-pressure limit, enhancing the rate 2-fold at 298 K but becoming negligible by 1000 K. The experimental rate measurements provide a critical test of the theoretical methods utilized to predict the reaction pathway for hydrocarbon

oxidation processes of increased complexity. The predicted thermal rate constants for a variety of processes on the  $C_6H_{11}O_2$  potential energy surface should prove useful in efforts to improve the fidelity of global models for cyclohexane oxidation processes.

# **Materials and Methods**

The methods utilized for IR action spectroscopy and time-resolved dynamics of reaction intermediates to OH radical products have been described previously.<sup>32, 43</sup> Cyclohexyl hydroperoxide (CHHP) has been prepared using a recently developed synthetic approach that avoids storage of large quantities of potentially explosive organic hydroperoxides, which is briefly described in SI and presented in detail in Ref. 45. Additional details on the experimental and theoretical methods are provided in SI. All data are available in the main text, supplementary materials, and Zenodo<sup>51</sup>, the latter of which contains the input for the Master Equation System Solver. Codes are available on GitHub or commercially, as detailed in SI.

Data, Materials, and Software Availability. Input for the Master Equation System Solver data have been deposited in Zenodo (10.5281/zenodo.10471648). All other data are included in the article and/or SI Appendix.

# **Acknowledgements and Funding Sources**

Research in the Lester laboratory was primarily supported by the US Department of Energy – Basic Energy Sciences under grant DE-FG02-87ER13792. Work at Argonne National Laboratory was supported by the US Department of Energy, Office of Science, Basic Energy Sciences, Division of Chemical Sciences, Geosciences, and Biosciences under contract No. DE-AC02-06CH11357. M.C.K. is grateful to the NSF (CHE-2102626) for the financial support of this research. Partial instrumentation support (NMR spectrometer) was provided by NSF CHE-1827457 and the Vagelos Institute for Energy Science and Technology. T.K.R. was primarily supported by a Walter-Benjamin Scholarship funded by the Deutsche Forschungsgemeinschaft (DFG, German Research Foundation) - Project number 508074809. This work used the Advanced Cyberinfrastructure Coordination Ecosystem: Service & Support (ACCESS) program, which is supported by National Science Foundation grants #2138259, #2138286, #2138307, #2137603, and #2138296, through the allocation TG-CHE190088. We thank William H. Green (MIT) for his thoughtful comments on the manuscript.

Author contributions: M.I.L. designed the research, Y.Q., T.K.R., A.W.J. and S.J.K. performed the research, C.A.S. and M.C.K. synthesized the cyclohexyl peroxide sample, Y.Q., T.K.R, A.W.J., S.J.K. and M.I.L. analyzed data, and S.J.K. and M.I.L. wrote the paper.

The authors declare no conflict of interest.

#### References

- 1. W. J. Pitz, C. J. Mueller, Recent progress in the development of diesel surrogate fuels. *Progr. Energy Combust. Sci.* **37**, 330-350 (2011).
- 2. S. M. Sarathy, G. Kukkadapu, M. Mehl, T. Javed, A. Ahmed, N. Naser, A. Tekawade, G. Kosiba, M. AlAbbad, E. Singh, S. Park, M. A. Rashidi, S. H. Chung, W. L. Roberts, M. A. Oehlschlaeger, C.-J. Sung, A. Farooq, Compositional effects on the ignition of FACE gasolines. *Combust. Flame* **169**, 171-193 (2016).
- 3. S. J. Eaton, S. H. Beis, S. A. Karunarathne, H. P. Pendse, M. C. Wheeler, Hydroprocessing of biorenewable thermal deoxygenation oils. *Energy Fuels* **29**, 3224-3232 (2015).
- 4. L. M. Balster, E. Corporan, M. J. DeWitt, J. T. Edwards, J. S. Ervin, J. L. Graham, S.-Y. Lee, S. Pal,
- D. K. Phelps, L. R. Rudnick, R. J. Santoro, H. H. Schobert, L. M. Shafer, R. C. Striebich, Z. J. West, G.
- R. Wilson, R. Woodward, S. Zabarnick, Development of an advanced, thermally stable, coal-based jet fuel. *Fuel Process. Technol.* **89**, 364-378 (2008).
- 5. R. Sommariva, R. S. Blake, R. J. Cuss, R. L. Cordell, J. F. Harrington, I. R. White, P. S. Monks, Observations of the Release of Non-methane Hydrocarbons from Fractured Shale. *Environ. Sci. Technol.* **48**, 8891-8896 (2014).
- 6. Y. Yang, A. L. Boehman, J. M. Simmie, Uniqueness in the low temperature oxidation of cycloalkanes. *Combust. Flame* **157**, 2357-2368 (2010).
- 7. Y. B. Lim, P. J. Ziemann, Effects of Molecular Structure on Aerosol Yields from OH Radical-Initiated Reactions of Linear, Branched, and Cyclic Alkanes in the Presence of NO<sub>x</sub>. *Environ. Sci. Technol.* **43**, 2328-2334 (2009).
- 8. J. F. Hunter, A. J. Carrasquillo, K. E. Daumit, J. H. Kroll, Secondary Organic Aerosol Formation from Acyclic, Monocyclic, and Polycyclic Alkanes. *Environ. Sci. Technol.* **48**, 10227-10234 (2014).
- 9. L. G. Jahn, D. S. Wang, S. V. Dhulipala, L. H. Ruiz, Gas-Phase Chlorine Radical Oxidation of Alkanes: Effects of Structural Branching, NO<sub>x</sub>, and Relative Humidity Observed during Environmental Chamber Experiments. *J. Phys. Chem. A* **125**, 7303-7317 (2021).
- 10. W. Hu, H. Zhou, W. Chen, Y. Ye, T. Pan, Y. Wang, W. Song, H. Zhang, W. Deng, M. Zhu, C. Wang, C. Wu, C. Ye, Z. Wang, B. Yuan, S. Huang, M. Shao, Z. Peng, D. A. Day, P. Campuzano-Jost, A. T. Lambe, D. R. Worsnop, J. L. Jimenez, X. Wang, Oxidation Flow Reactor Results in a Chinese Megacity Emphasize the Important Contribution of S/IVOCs to Ambient SOA Formation. *Environ. Sci. Technol.* **56**, 6880-6893 (2022).
- 11. T. Chatterjee, M. Wang, S. W. Wagnon, G. Kukkadapu, C.-J. Sung, W. J. Pitz, Autoignition of cyclohexane at low-to-intermediate temperatures: Rapid compression machine experiments and improved comprehensive chemical kinetic model. *Combust. Flame* **259**, 113187 (2024) and references cited therein.
- 12. J. Platz, J. Sehested, O. J. Nielsen, T. J. Wallington, Atmospheric Chemistry of Cyclohexane: UV Spectra of c-C<sub>6</sub>H<sub>11</sub> and (c-C<sub>6</sub>H<sub>11</sub>)O<sub>2</sub> Radicals, Kinetics of the Reactions of (c-C<sub>6</sub>H<sub>11</sub>)O<sub>2</sub> Radicals with NO and NO<sub>2</sub>, and the Fate of the Alkoxy Radical (c-C<sub>6</sub>H<sub>11</sub>)O. J. Phys. Chem. A **103**, 2688-2695 (1999).
- 13. S. M. Aschmann, J. Arey, R. Atkinson, Reactions of OH Radicals with C<sub>6</sub>–C<sub>10</sub> Cycloalkanes in the Presence of NO: Isomerization of C<sub>7</sub>–C<sub>10</sub> Cycloalkoxy Radicals. *J. Phys. Chem. A* **115**, 14452-14461 (2011).
- 14. C. Cavallotti, R. Rota, T. Faravelli, E. Ranzi, Ab initio evaluation of primary cyclo-hexane oxidation reaction rates. *Proc. Combust. Inst.* **31**, 201-209 (2007).

- 15. A. M. Knepp, G. Meloni, L. E. Jusinski, C. A. Taatjes, C. Cavallotti, S. J. Klippenstein, Theory, measurements, and modeling of OH and HO<sub>2</sub> formation in the reaction of cyclohexyl radicals with O<sub>2</sub>. *Phys. Chem. Chem. Phys.* **9**, 4315-4331 (2007).
- 16. B. Sirjean, P. A. Glaude, M. F. Ruiz-Lòpez, R. Fournet, Theoretical kinetic study of the reactions of cycloalkylperoxy radicals. *J. Phys. Chem. A* **113**, 6924-6935 (2009).
- 17. J. Zou, Y. Li, L. Ye, H. Jin, A comprehensive study on low-temperature oxidation chemistry of cyclohexane. I. Conformational analysis and theoretical study of first and second oxygen addition. *Combust. Flame* **235**, 111658 (2022).
- 18. J. Zou, H. Jin, D. Liu, X. Zhang, H. Su, J. Yang, A. Farooq, Y. Li, A comprehensive study on low-temperature oxidation chemistry of cyclohexane. II. Experimental and kinetic modeling investigation. *Combust. Flame* **235**, 111550 (2022).
- 19. J. Bourgalais, H.-H. Carstensen, O. Herbinet, G. A. Garcia, P. Arnoux, L.-S. Tran, G. Vanhove, L. Nahon, M. Hochlaf, F. Battin-Leclerc, Product identification in the low-temperature oxidation of cyclohexane using a jet-stirred reactor in combination with SVUV-PEPICO analysis and theoretical quantum calculations. *J. Phys. Chem. A* **126**, 5784-5799 (2022).
- 20. J. J. Orlando, G. S. Tyndall, Laboratory studies of organic peroxy radical chemistry: an overview with emphasis on recent issues of atmospheric significance. *Chem. Soc. Rev.* **41**, 6294-6317 (2012).
- 21. M. Demireva, L. Sheps, N. Hansen, Insights into constraining rate coefficients in fuel oxidation mechanisms using genetic algorithm optimization. *Energy Fuels* **37**, 14240–14253 (2023).
- 22. J. Zádor, C. A. Taatjes, R. X. Fernandes, Kinetics of elementary reactions in low-temperature autoignition chemistry. *Prog. Energy Combust. Sci.* **37**, 371-421 (2011).
- 23. D. L. Osborn, Reaction mechanisms on multiwell potential energy surfaces in combustion (and atmospheric) chemistry. *Annu. Rev. Phys. Chem.* **68**, 233-260 (2017).
- 24. Z. Wang, O. Herbinet, N. Hansen, F. Battin-Leclerc, Exploring hydroperoxides in combustion: History, recent advances and perspectives. *Prog. Energy Combust. Sci.* **73**, 132-181 (2019).
- 25. F. Paulot, J. D. Crounse, H. G. Kjaergaard, A. Kürten, J. M. St. Clair, J. H. Seinfeld, P. O. Wennberg, Unexpected epoxide formation in the gas-phase photooxidation of isoprene. *Science* **325**, 730-733 (2009).
- 26. J. Peeters, J.-F. Müller, T. Stavrakou, V. S. Nguyen, Hydroxyl radical recycling in isoprene oxidation driven by hydrogen bonding and hydrogen tunneling: The upgraded LIM1 mechanism. *J. Phys. Chem. A* **118**, 8625-8643 (2014).
- 27. M. Ehn, J. A. Thornton, E. Kleist, M. Sipilä, H. Junninen, I. Pullinen, M. Springer, F. Rubach, R. Tillmann, B. Lee, F. Lopez-Hilfiker, S. Andres, I.-H. Acir, M. Rissanen, T. Jokinen, S. Schobesberger, J. Kangasluoma, J. Kontkanen, T. Nieminen, T. Kurtén, L. B. Nielsen, S. Jørgensen, H. G. Kjaergaard, M. Canagaratna, M. D. Maso, T. Berndt, T. Petäjä, A. Wahner, V.-M. Kerminen, M. Kulmala, D. R. Worsnop, J. Wildt, T. F. Mentel, A large source of low-volatility secondary organic aerosol. *Nature* 506, 476-479 (2014).
- 28. T. Berndt, B. Mentler, W. Scholz, L. Fischer, H. Herrmann, M. Kulmala, A. Hansel, Accretion product formation from ozonolysis and OH radical reaction of  $\alpha$ -pinene: Mechanistic insight and the Influence of isoprene and ethylene. *Environ. Sci. Technol.* **52**, 11069-11077 (2018).
- 29. K. H. Møller, T. Kurtén, K. H. Bates, J. A. Thornton, H. G. Kjaergaard, Thermalized epoxide formation in the atmosphere. *J. Phys. Chem. A* **123**, 10620-10630 (2019).
- 30. E. L. D'Ambro, S. Schobesberger, C. J. Gaston, F. D. Lopez-Hilfiker, B. H. Lee, J. Liu, A. Zelenyuk, D. Bell, C. D. Cappa, T. Helgestad, Z. Li, A. Guenther, J. Wang, M. Wise, R. Caylor, J. D. Surratt, T. Riedel, N. Hyttinen, V. T. Salo, G. Hasan, T. Kurtén, J. E. Shilling, J. A. Thornton, Chamber-based

- insights into the factors controlling epoxydiol (IEPOX) secondary organic aerosol (SOA) yield, composition, and volatility. *Atmos. Chem. Phys.* **19**, 11253-11265 (2019).
- 31. J. D. Savee, E. Papajak, B. Rotavera, H. Huang, A. J. Eskola, O. Welz, L. Sheps, C. A. Taatjes, J. Zádor, D. L. Osborn, Direct observation and kinetics of a hydroperoxyalkyl radical (QOOH). *Science* **347**, 643-646 (2015).
- 32. A. S. Hansen, T. Bhagde, K. B. Moore, D. R. Moberg, A. W. Jasper, Y. Georgievskii, M. F. Vansco, S. J. Klippenstein, M. I. Lester, Watching a hydroperoxyalkyl radical (•QOOH) dissociate. *Science* 373, 679-682 (2021).
- 33. T. Bhagde, A. S. Hansen, S. Chen, P. J. Walsh, S. J. Klippenstein, M. I. Lester, Energy-resolved and time-dependent unimolecular dissociation of hydroperoxyalkyl radicals (•QOOH). *Faraday Discuss.* **238**, 575-588 (2022).
- 34. J. Bugler, J. Power, H. J. Curran, A theoretical study of cyclic ether formation reactions. *Proc. Combust. Inst.* **36**, 161-167 (2017).
- 35. C. F. Goldsmith, W. H. Green, S. J. Klippenstein, Role of O<sub>2</sub> + QOOH in low-temperature ignition of propane. 1. temperature and pressure dependent rate coefficients. *J. Phys. Chem. A* **116**, 3325-3346 (2012).
- 36. A. Miyoshi, Systematic Computational Study on the Unimolecular Reactions of Alkylperoxy (RO<sub>2</sub>), Hydroperoxyalkyl (QOOH), and Hydroperoxyalkylperoxy (O<sub>2</sub>QOOH) Radicals. *J. Phys. Chem. A* **115**, 3301-3325 (2011).
- 37. R. X. Fernandes, J. Zádor, L. E. Jusinski, J. A. Miller, C. A. Taatjes, Formally direct pathways and low-temperature chain branching in hydrocarbon autoignition: the cyclohexyl + O<sub>2</sub> reaction at high pressure. *Phys. Chem. Chem. Phys.* **11**, 1320-1327 (2009).
- 38. J. Zádor, H. Huang, O. Welz, J. Zetterberg, D. L. Osborn, C. A. Taatjes, Directly measuring reaction kinetics of 'QOOH a crucial but elusive intermediate in hydrocarbon autoignition. *Phys. Chem. Chem. Phys.* **15**, 10753-10760 (2013).
- 39. C. A. Whelan, M. A. Blitz, R. Shannon, L. Onel, J. P. Lockhart, P. W. Seakins, D. Stone, Temperature and pressure dependent kinetics of QOOH decomposition and reaction with O<sub>2</sub>: Experimental and theoretical investigations of QOOH radicals derived from Cl + (CH<sub>3</sub>)<sub>3</sub>COOH. *J. Phys. Chem. A* **123**, 10254-10262 (2019).
- 40. E. J. Silke, W. J. Pitz, C. K. Westbrook, M. Ribaucour, Detailed chemical kinetic modeling of cyclohexane oxidation. *J. Phys. Chem. A* **111**, 3761-3775 (2007).
- 41. J. M. Anglada, R. Crehuet, J. S. Francisco, The stability of  $\alpha$ -hydroperoxyalkyl radicals. *Chem. Eur. J.* **22**, 18092-18100 (2016).
- 42. Z. Serinyel, O. Herbinet, O. Frottier, P. Dirrenberger, V. Warth, P. A. Glaude, F. Battin-Leclerc, An experimental and modeling study of the low- and high-temperature oxidation of cyclohexane. *Combust. Flame* **160**, 2319-2332 (2013).
- 43. F. Liu, J. M. Beames, A. S. Petit, A. B. McCoy, M. I. Lester, Infrared-driven unimolecular reaction of CH<sub>3</sub>CHOO Criegee intermediates to OH radical products. *Science* **345**, 1596-1598 (2014).
- 44. A. S. Hansen, T. Bhagde, Y. Qian, A. Cavazos, R. M. Huchmala, M. A. Boyer, C. F. Gavin-Hanner, S. J. Klippenstein, A. B. McCoy, M. I. Lester, Infrared spectroscopic signature of a hydroperoxyalkyl radical (•QOOH). *J. Chem. Phys.* **156**, 014301 (2022).
- 45. T. K. Roy, Y. Qian, E. Karlsson, R. Rabayah, C. A. Sojdak, M. C. Kozlowski, T. N. V. Karsili, M. I. Lester, Vibrational Spectroscopy and Dissociation Dynamics of Cyclohexyl Hydroperoxide. (submitted).

- 46. Y. Fang, F. Liu, V. P. Barber, S. J. Klippenstein, A. B. McCoy, M. I. Lester, Communication: Real time observation of unimolecular decay of Criegee intermediates to OH radical products. *J. Chem. Phys.* **144**, 061102 (2016).
- 47. V. D. Knyazev, Reactivity Extrapolation from Small to Large Molecular Systems via Isodesmic Reactions for Transition States. *J. Phys. Chem. A* **108**, 10714-10722 (2004).
- 48. S. N. Elliott, M. Keçeli, M. K. Ghosh, K. P. Somers, H. J. Curran, S. J. Klippenstein, High-accuracy heats of formation for alkane oxidation: From small to large via the automated CBH-ANL method. *J. Phys. Chem. A* **127**, 1512-1531 (2023).
- 49. A. W. Jasper, K. M. Pelzer, J. A. Miller, E. Kamarchik, L. B. Harding, S. J. Klippenstein, Predictive a priori pressure-dependent kinetics. *Science* **346**, 1212-1215 (2014).
- 50. A. W. Jasper, Microcanonical rate constants for unimolecular reactions in the low-pressure limit. *J. Phys. Chem. A* **124**, 1205-1226 (2020).
- 51. Y. Qian et al., Isomer-resolved Unimolecular dynamics of the hydroperoxyalkyl intermediate (•QOOH) in cyclohexane oxidation. 10.5281/zenodo.10471648 (2024).